Chemically Modified Solid-State Nanopores

Meni Wanunu and Amit Meller*

Departments of Biomedical Engineering and Physics, Boston University, Boston, Massachusetts 02215

ABSTRACT

Nanopores are extremely sensitive single-molecule sensors. Recently, electron beams have been used to fabricate synthetic nanopores in thin solid-state membranes with subnanometer resolution. Here we report a new class of chemically modified nanopore sensors. We describe two approaches for monolayer coating of nanopores: (1) self-assembly from solution, in which nanopores ∼10 nm diameter can be reproducibly coated, and (2) self-assembly under voltage-driven electrolyte flow, in which we are able to coat 5 nm nanopores. We present an extensive characterization of coated nanopores, their stability, reactivity, and pH response.

Nanopores have emerged in recent years as versatile single-molecule detectors. The sensing principle is based on transient interruptions in the ion-current of an electrolyte, induced by the entry, transport, and exit of a particular analyte from the pore. A distinguishing feature of nanopores is that they can be used to analyze not only small molecules but also long biopolymers, such as DNA and RNA, with resolution on the order of the nanopore length (several nanometers). A well-studied system involves the lipid-embedded α-hemolysin (α-HL) protein pore, which can accommodate various types of biopolymers. α-HL has been used extensively to discriminate between DNA and RNA sequences, to study DNA unzipping kinetics, orientation of entry, DNA−protein interactions, and peptide transport.[1] An important outcome of these studies has been the realization that threaded biopolymer dynamics is governed by its *interactions* with the nanopore walls.[2] This notion was utilized for the detection of small molecules, metal ions, and the discrimination of enantiomer drugs, by employing molecular biology methods to modify the α-HL nanopore.[3] However, the range of sensing applications using α-HL is limited by its fixed dimensions and the delicate lipid membrane.

To expand the realm of nanopore sensing, synthetic nanopores have recently been introduced using a variety of materials, such as polymers,[4,5] glass,[6] and thin solid-state membranes.[7−10] Such nanopores have demonstrated utility for sensing single-stranded[11,12] and double-stranded[7,11,13] DNA, ions,[14] macromolecules,[15] and proteins.[16,17] Nanopores incorporated in thin (∼10 nm) solid-state inorganic membranes are highly promising materials, since the nanopore volume can be reduced to a few nanometers in *all* dimensions, on par with biological membrane channels. In addition, the planar geometry permits high-resolution fabrication and characterization using the transmission electron microscope (TEM), as exemplified by subnanometer size control for nanopores down to 1 nm diameters.[7,8,10,11] Further, the fabrication of high-density nanopore arrays is possible,[10,18] setting the stage for high-throughput biomolecular analysis, in particular ultrafast DNA sequencing.

Nanoscale control over the surface properties of nanopores can govern its interactions with various analytes, resulting in "smart" nanopore sensors. Various approaches for nanopore functionalization have been reported, from deposition of metals[19] and oxides[20,21] to various organic modifications.[16,21,22] However, the resulting nanopore structure often gains significant thickness, and in some cases the morphology is unknown, due to unavailability of imaging methods. In particular, molecular coating of solid-state nanopores approaching the nanometer scale *in all dimensions* has not been reported to date. In this paper, we introduce robust procedures for chemical modification of nanopores of sizes 5−20 nm fabricated in thin SiN membranes. We adopt well-established self-assembly methods to control the chemical and physical properties of a single nanopore, such as its charge, polarity, pH sensitivity, etc. We introduce a novel method for reproducible coating of nanopores as small as 5 nm and present results that demonstrate surface modification, fast reaction kinetics, and pH responsiveness. Our methods broadly expand the utility of nanopores for biological sensing: Dressing an inorganic pore surface with a variety of organic coatings not only makes it more biologically friendly but further allows control of surface charge, hydrophobicity, and chemical functionality. We demonstrate
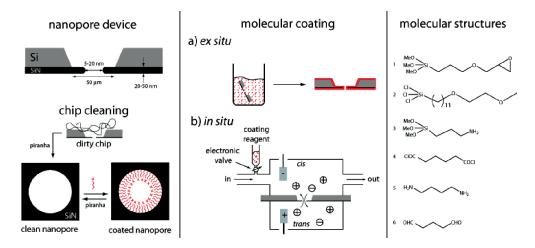
* Corresponding author. E-mail: ameller@bu.edu.

Figure 1. (left panel) A schematic picture of the nanopore device. Piranha solution is used to clean the nanopore surfaces before coating with organosilanes, as well as to "uncoat" the nanopores. (middle panel) A depiction of two schemes for coating nanopores. In the *ex situ* method, the activated nanopore is simply immersed in silane solution, followed by cleaning steps (not shown). In the *in situ* method, the nanopore device is assembled in a two-chamber cell and a voltage is applied across it, driving supporting electrolyte through the pore during the silane deposition process. (right panel) Structures of the molecules used for various coatings. Molecules **1**–**3** are organosilanes, while **4**–**6** are used in further reactions with functional silane monolayers.

an ultrasensitive single nanopore pH sensor operating at physiological ionic strengths.

Our solid-state nanopore device is depicted in Figure 1 (left panel). The SiN membrane surface contains a native oxide layer,[23] which is used here for monolayer self-assembly of organosilanes.[24] Prior to coating, we find that piranha treatment is crucial for removal of contaminants and surface activation. Further, the coating procedures we describe are reversible: piranha treatment can be used to completely remove the organic coatings and regenerate the clean nanopore surface. The middle panel in Figure 1 shows two alternative molecular coating approaches: (a) *ex situ* assembly, in which the organic coating is performed by immersion of the nanopore chip into the deposition solution; (b) *in situ* assembly, in which organic molecules are allowed to react with the nanopore surface under driven electrolyte flow. While the *ex situ* coating method is more straightforward, we find that the *in situ* assembly allows us to coat smaller nanopores without clogging, down to 5 nm. On the right panel in Figure 1, we show the molecules used for coating the nanopores. Films designated with a "+" sign were prepared by multiple reaction steps. We chose to investigate coatings with common functional groups: Epoxy (**1**), methoxyethylene glycol ("PEG"-type) (**2**), amine (**3**, **3** + **5**), carboxylic acid (**3** + **4**), and aldehyde (**6**). Molecules **1**–**3** are organosilanes, which directly self-assemble on the nanopore surface to form functional monolayers. Molecules **4** and **6** were used to convert amine-coated surfaces to carboxylic acid and aldehydes, respectively. Molecule **5** was used in further reaction with the (**3** + **4**) surface to generate a thicker amine coating (see Supporting Information).

We investigated the film thickness, roughness, and chemical composition of the different films on planar SiN substrates by ellipsometry, noncontact atomic force microscopy (AFM), and X-ray photoelectron spectroscopy (XPS). In Table 1, we compare the ellipsometric thickness, δ, with the calculated thickness based on molecular models. We note

Table 1. Characterization of the Molecular Films on SiN Substrates Using Ellipsometry

film	$n_f{}^a$ @ 633 nm	δ (nm)	model thickness[b] (nm)
1	1.43	1.4 ± 0.1	1.1
2	1.46	2.5 ± 0.2	2.2
3	1.50	0.6 ± 0.1	0.7
3 + 4	1.50	1.2 ± 0.2	1.4
3 + 4 + 5	1.50	1.7 ± 0.2	2.1
3 + 6	1.50	1.1 ± 0.2	1.3

[a] Based on bulk refractive index values. [b] Calculated from molecular models (CS Chem3D), assuming upright orientation on the surface.

that the measured thicknesses are in agreement with calculated values for films **1**–**3**, indicating the formation of homogeneous monolayers on the SiN substrate. Moreover, the increase in film thickness upon the addition of **4** or **6** suggests that the amine group remains reactive on the surface. Further, reaction of the terminal carbonyl chloride (**3** + **4**) with diamine **5** was successful. AFM characterization on these films yielded root mean square roughness values in the range 0.4–0.7 nm, similar to uncoated SiN (0.58 nm), implying a homogeneous film distribution.

XPS measurements were performed to validate the chemical identity of the coated films. Figure 2 compares bare (piranha-treated) SiN to films **1** and (**3** + **4** + **5**). The SiN exhibits strong signals for Si, N, and O, as well as a residual C signal, attributed to contamination. Following coating with **1** (middle curve), we observe the reduction of signals for Si, O, and N, coupled with an increase of the C signal.[25] The amino-terminated film (**3** + **4** + **5**) exhibits a second N peak at 402 eV (see arrow), corresponding to a protonated amine state on the film ($NH_3{}^+$).[26]

The coating of highly concave surfaces in confined volume is considerably different than coating of flat surfaces described above. Not only do the concave surfaces induce different molecular packing, the highly confined volume of
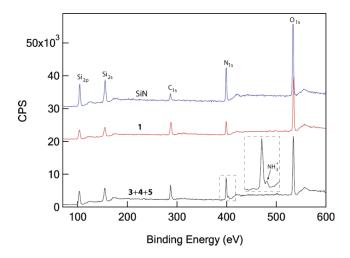
Figure 2. XPS spectra of bare SiN films on Si (top) and the same substrates after coating with **1** (middle) and (**3** + **4** + **5**) (bottom). A peak at 402 eV (see inset) is attributed to the presence of ammonium (NH_3^+) ions in the film (**3** + **4** + **5**) (from ref 26). The middle and the top curves were shifted by 20×10^3 and 30×10^3 counts/s, respectively.

Table 2. Ion Conductance at 1 M KCl, pH 8.5, for Bare and Coated Nanopores (n = Number of Trials)

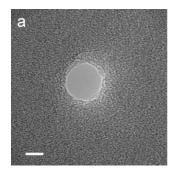| coating	D_{bare} (nm)	G_{bare} (nS)	G_{coated} (nS)	$\langle d_{eff} \rangle$ (nm)[a]	d' (nm)[b]
1	13 ($n = 2$)	75 ± 4	35 ± 4	9.5	10
	10 ($n = 5$)	34 ± 4	20 ± 5	7	7
2	15 ($n = 2$)	120 ± 5	26 ± 3	9	10
	10 ($n = 2$)	34 ± 4	13 ± 4	6	6
3	14 ($n = 2$)	100 ± 5	55 ± 8	12	12.5
	12 ($n = 10$)	65 ± 4	45 ± 5	11	10.5
3 + 4 + 5	25 ($n = 1$)	250	110	18	21
	10 ($n = 1$)	31	9	5	6
3 + 6	12 ($n = 10$)	65 ± 4	29 ± 7	9	9.5
	10 ($n = 1$)	33	8	5	7.5

[a] Average error in all values is $\pm 10\%$. [b] Based on the ellipsometric thickness (see text).

the nanopore may alter the adsorption kinetics. Furthermore, the characterization techniques described above cannot be used to probe coating inside a nanopore. On the other hand, the ion flux through the nanopores should be extremely sensitive to the nanopore coating thickness, since the ionic conductance (G) depends quadratically, to a first approximation, on the pore diameter, d. To validate this, we performed an extensive series of ion-conductance measurements for uncoated and coated pores using nanopores with diameters in the range $10-25$ nm (Table 2). We measured G for each chip before and after the coating procedure and estimated the effective diameter, d_{eff}, based on the G values. We compare these numbers with the model coated nanopore size, $d' = d_{bare} - 2\delta$, where d_{bare} is the TEM measured diameter of the uncoated pore and δ is the coating thickness measured by ellipsometry. An agreement between d_{eff} and d' would indicate that nanopore coating thickness is commensurate with surface coating thickness. As seen in Table 2, the effective nanopore sizes agree very well with the model size for *all* the coating types we used, supporting the formation of monolayers with the expected thickness inside the

nanopores. A reduction in G may also be attributed to an increase of the membrane thickness. However, only a negligible contribution is expected from this: On the 50 nm thick SiN membrane used in these measurements, the thickest coating (2.5 nm) should increase the membrane thickness by 10% (5 nm) and in turn should decrease G by 10% or less. In contrast, we observe a roughly 80% decrease in G for this coating, implying that the reduction in G is primarily due to coating inside the nanopore.

Table 2 also demonstrates the reversible nature of our coating procedures. For example, in coating **1**, the same nanopores were cycled five times through piranha/coating treatment cycles, giving rise to distinct conductance values of the bare and chemically modified nanopore, with ∼10% variations.

Nanopore coating is further supported by high-resolution TEM imaging. Figure 3a displays a TEM image of a piranha-treated nanopore (10 nm). Figure 3b displays a similar 10 nm pore after coating with the 1.7 nm thick (**3** + **4** + **5**) layer. We note several marked differences: First, the coated surface displays larger grains. Second, the nanopore boundary appears dull, as opposed to the sharp SiN/pore boundary in the unmodified nanopore. The nanopore interior in the TEM image reveals an uneven grayish decoration (indicated by an arrow), attributed to coating. This layer is clearly in focus, marked by the sharp boundary between the coating and vacuum. The maximum estimated coating thickness is ∼2 nm, very close to the measured coating thickness (1.7 nm). The image on the right in Figure 3b displays a TEM image of the nanopore following a 30 s exposure to the e-beam under imaging conditions (e-beam intensity ∼10^3 e/nm² s). Clearly, the surface graininess disappeared—highly resembling the uncoated membrane in Figure 3a. This is in line with destruction of the organic film. We can exclude the possibility that these changes are caused by changes to the SiN membrane, since nanopores in SiN are fabricated using a highly focused electron beam of intensity ∼10^9 e/nm² s, and their final size shaped with an intensity of 10^6 e/nm² s.[8,10] Under imaging intensities ($<10^3$ e/nm² s), we and others[8] have not been able to observe changes in nanopore structure over extended imaging periods (minutes). In contrast, low-intensity e-beams are known to destroy thin *organic* films.[27]

While the *ex situ* coating procedure is highly reliable for nanopores larger than ∼10 nm, we find that smaller pores tend to clog, possibly due to accumulation of silane molecules inside the pore. To circumvent this problem, we introduce an *in situ* coating method (Figure 1b). In this approach, we mix the silane with organic electrolyte in anhydrous solvent, and apply a voltage across the nanopore during the deposition process. The electric field induces flow of electrolyte across the nanopore, effectively mobilizing non-specifically bound molecules. Our technique is illustrated in Figure 4, in which the coating of a 5 nm pore with aminosilane **3** is monitored over time. We used anhydrous MeOH as the solvent and 0.5 M tetrabutylammonium chloride (TBACl) as the supporting electrolyte. The injection of **3** at 50 s (arrow 1) resulted in a nearly exponential
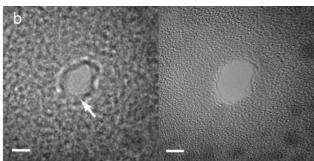
Figure 3. (a) Bright-field TEM images of a 10 nm nanopore following cleaning with piranha solution. (b, left) TEM image of a 10 nm nanopore following coating with (**3** + **4** + **5**). The arrow indicates the grayish region, which corresponds to the nanopore coating. (right) TEM image of the same pore after 30 s of irradiation under low e-beam dose, during which the organic layer appears to have been removed. The scale bar in all images is 5 nm.
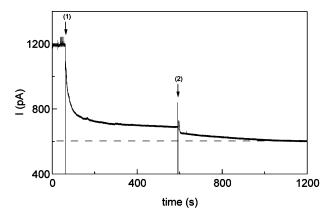

Figure 4. Current−time trace (measured at 400 mV) for the in situ coating of a 5 nm nanopore using aminosilane **3** (supporting electrolyte, 0.5 M TBACl; solvent, anhydrous MeOH). Equal aliquots of **3** were injected at points 1 and 2.

decrease in the current from 1.2 nA down to ∼0.7 nA, with a characteristic time scale of 17 s. The addition of an equal aliquot of **3** at 600 s (arrow 2) caused only a minor decrease in the current, from 0.7 to ∼0.6 nA. We interpret this result as follows: The first aliquot of **3** resulted in monolayer deposition on the pore surface. On the basis of the molecular thickness of **3** (0.7 nm, see Table 1), we expect that a single monolayer would decrease the pore cross-sectional area by 48%. This value is in excellent agreement with the measured reduction in current of 42%. The minor additional decrease in the current after the second addition of **3** is attributed to dilution of the electrolyte by the uncharged silane. Similar results were obtained in repeated measurements.

Amine-modified surfaces are versatile platforms for a wide range of applications in biotechnology. For example, glutaraldehyde (**6**) is a common reagent used for coupling amine-modified surfaces with proteins.[28] We tested coated nanopore functionality by monitoring the reaction of our amine-coated nanopores with glutaraldehyde. Figure 5a displays an ion-current trace (measured in 1 M KCl aqueous solution, pH 5.8) of a 12 nm nanopore precoated with aminosilane **3**. Upon the addition of **6** at $t = 0$ (to a final concentration of 2%), G quickly drops by ∼50% and stabilizes at a level of ∼ 1.5 nA (II). To show that the current reduction is specifically due to reaction with the amine-coated nanopore, we display a current trace measured during the
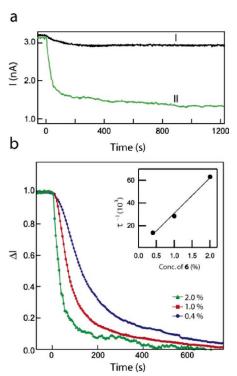

Figure 5. (a) Current−time traces (measured at 100 mV) for the addition of 2% **6** to the cis chamber of a bare 10 nm (I) and amine-coated 12 nm nanopore (II). (b) Normalized change in the ion-current (measured at 100 mV, 1 M KCl buffered with 10 mM phosphate to pH 5.8) of 12 nm diameter nanopores coated with aminosilane **3** upon the addition of gluteraldehyde (**6**) to final concentrations of 0.4% (a), 1% (b), and 2% (c) in the cis-chamber (at $t = 0$). The bulk conductivities of the GA solutions were adjusted in order to match that of the electrolyte (161 ± 1 mS). Inset: Time constant (τ^{-1}) fitting results to first-order adsorption kinetics for the different concentrations. The solid line is a best fit to the data.

addition of 2% **6** to an *uncoated* 10 nm pore (I), which resulted in only 6% change in G. This illustrates the specificity of the glutaraldehyde reaction on amine-coated pores.

The reaction kinetics inside an amine-coated nanopore also shows dependence on the bulk concentration of **6**. In Figure 5b, we present three ion-current traces obtained during addition of **6** at bulk concentrations of 2.0%, 1.0%, and 0.4% v/v. These curves were fitted to first-order adsorption kinetics, yielding a linear dependence on concentration
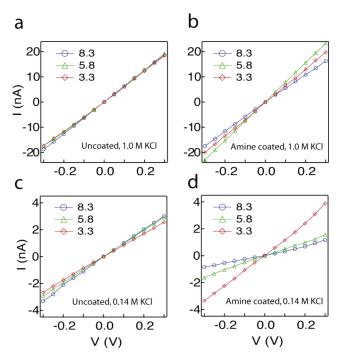
Figure 6. $I-V$ curves in 1.0 M KCl for 12 nm pores at indicated pH levels before (a) and after (b) APTMS coating. (c and d) $I-V$ curves at 0.14 M KCl for the same uncoated and coated nanopores. The coated pore conductance shows high pH sensitivity at the low ionic strength level (d), whereas uncoated pores do not display a measurable dependence at both ionic strengths, suggesting negligible changes in the surface charge.

(inset). In all cases, the steady-state ion-current levels after the addition of **6** were $50 \pm 10\%$ of the initial pore currents.

Aside from the bulk concentration of ions, surface charges may also affect ion transport through nanoscale channels. Charged surfaces should raise the nanopore conductance by mediating transport of counterions near the pore walls.[29,30] To investigate this effect in our nanopores, we use the fact that amino groups can be protonated upon lowering the solution pH. Since surface ammonium pK_a values are lower ($pK_a \sim 5-6$) than those in solution ($pK_a \sim 9$),[31] we expect to observe a strong ion conductance pH dependence around pH 5–6. In Figure 6, we present $I-V$ curves of an uncoated nanopore (a) and an amine-coated nanopore (b), at 1.0 M KCl and at pH 3.3, 5.8, and 8.3. Similar measurements at 0.14 M KCl are shown in (c) and (d). At 1.0 M KCl, both coated and uncoated pores exhibit a weak pH dependence on conductance. In contrast, at 0.14 M KCl, the coated pore displays a marked current enhancement ($\sim$4-fold) upon lowering the pH from 8.3 to 3.3, while the uncoated pore still remains insensitive to pH. To explain the marked pH sensitivity of the coated pores, we write the pore current as

$$I \approx \frac{\pi d^2}{4}\sigma_B\left(1 + 4\frac{\lambda_D}{d}\epsilon\right) \tag{1}$$

where σ_B is the bulk mobilities of the KCl ions, λ_D the Debye length (effective double-layer thickness), and $\epsilon = (\sigma_S - \sigma_B/\sigma_B)$ is the mobility enhancement (or reduction) near the surface. At 1.0 M KCl, λ_D is roughly 0.3 nm; thus $(\lambda_D/d) \ll$

1 and surface effects are small. On the other hand, at 0.14 M KCl, $\lambda_D \sim 1$ nm, thus $(\lambda_D/d) \sim 0.1$, leading to a significant pH dependence on the ion conductance for the coated pore. Our results are in agreement with measurements performed in track-etched PETP pores, which have native carboxylic groups on their surface.[4] Our finding that the conductance of uncoated pores is independent of pH strongly indicates a similar surface charge at this pH range for our nanopores. Reported surface pK_a values for SiO_2 surfaces widely vary,[32] perhaps influenced by the exact form of SiO_2 and the measurement conditions. In a similar range of pH values, Stein and co-workers have observed $\sim$60% enhancement in the conductance for $\sim$400 nm wide amine-modified channels etched in glass, roughly 2 orders of magnitude larger than our nanopores.[29] According to eq 1, in order to observe a similar current enhancement, the required ionic strength would be $\sim$4 orders of magnitude smaller ($\lambda_D \sim I^{-(1/2)}$, where I is the ionic strength) than in our experiment, or roughly 10^{-5} M. This value is indeed close to the molar concentration used in ref 29, for which measurable pH effects were observed.

In conclusion, we have presented *ex situ* and *in situ* methods for nanopore functionalization using self-assembly of organosilane molecules. A number of analytical methods have been employed to clearly demonstrate (A) monolayer coating of various chemical groups inside >10 nm pores fabricated in SiN membranes and (B) ion-current through the coated nanopores closely correlates with the coating thickness. *In situ* measurements were used to probe the coating kinetics in real time. In this paper we focused on amine-terminated groups, due to their wide range of applicability. We show that a second, selective layer, can be formed on amine-coated pores and that the adsorption kinetics can be observed by monitoring the ion-current flowing through single nanopores. We note that the characteristic adsorption time scale is comparable with bulk adsorption onto planar surfaces, suggesting high reactivity on the nanopore surface.

We find that the coated nanopore is stable over days, even under treatments with voltage pulses of up to 5 V. This result is encouraging, considering the fact that silane monolayers can degrade under *in vitro* solution conditions.[33] High bandwidth (100 kHz) measurements of the coated and uncoated nanopores yielded similar noise values. Amine-coated nanopores exhibit pH sensitive conductance, similar to previously reported effects. However, due to the small dimensions of our nanopores, we are able to observe 4-fold difference in the conductance at physiological ionic strengths (0.14 M). Coated nanoscale pores can thus be used to fabricate ultrasmall and sensitive pH sensors. Chemically modified nanopores fabricated in inorganic membranes open a wide range of possibilities for stochastic sensing. For example, amine-terminated groups can be used to immobilize protein receptors in a robust, nearly two-dimensional device. Our planar geometry allows straightforward multiplexing using nanopore arrays. In future work, we will explore the possibility of using chemically modified nanopores to control

the dynamics of biopolymer transport and to introduce analyte-specific groups into the nanopore.

Supporting Information Available: A detailed Experimental Section for the characterization and nanopore coating methods. This material is available free of charge via the Internet at http://pubs.acs.org.

References

(1) (a) Kasianowicz, J. J.; Brandin, E.; Branton, D.; Deamer, D. W. *Proc. Natl. Acad. Sci. U.S.A.* **1996**, *93*, 13770−13773. (b) Akeson, M.; Branton, D.; Kasianowicz, J. J.; Brandin, E.; Deamer, D. W. *Biophys. J.* **1999**, *77*, 3227−3233. (c) Meller, A.; Nivon, L.; Brandin, E.; Golovchenko, J.; Branton, D. *Proc. Natl. Acad. Sci. U.S.A.* **2000**, *97*, 1079−1084. (d) Meller, A.; Nivon, L.; Branton, D. *Phys. Rev. Lett.* **2001**, *86*, 3435−3438. (e) Sauer-Budge, A. F.; Nyamwanda, J. A.; Lubensky, D. K.; Branton, D. *Phys. Rev. Lett.* **2003**, *90*, 238101. (f) Mathé, J.; Visram, H.; Viasnoff, V.; Rabin, Y.; Meller, A. *Biophys. J.* **2004**, *87*, 3205−3212. (g) Mathé, J.; Aksimentiev, A.; Nelson, D. R.; Schulten, K.; Meller, A. *Proc. Natl. Acad. Sci. U.S.A.* **2005**, *102*, 12377−122382. (h) Butler, T. Z.; Gundlach, J. H.; Troll, M. A. *Biophys. J.* **2006**, *90*, 190−199. (i) Stefureac, R.; Long, Y. T.; Kraatz, H. B.; Howard, P.; Lee, J. S. *Biochemistry* **2006**, *45*, 9172−9179. (j) Hornlower, B.; Coombs, A.; Whitaker, R. D.; Kolomeisky, A.; Picone, S. J.; Meller, A.; Akeson, M. *Nat. Methods* **2007**, *4*, 315−317.

(2) Meller, A. *J. Phys.*: *Condens. Matter* **2003**, *15*, R581−R607.

(3) (a) Bayley, H.; Cremer, P. *Nature* **2001**, *413*, 226−230. (b) Braha, O.; Gu, L. Q.; Zhou, L.; Lu, X.; Cheley, S.; Bayley, H. *Nat. Biotechnol.* **2000**, *18*, 1005−1007. (c) Gu, L. Q.; Braha, O.; Conlan, S.; Cheley, S.; Bayley, H. *Nature* **1999**, *398*, 686−690. (d) Howorka, S.; Cheley, S.; Bayley, H. *Nat. Biotechnol.* **2001**, *19*, 636−639. (e) Cheley, S.; Gu, L. Q.; Bayley, H. *Chem. Biol.* **2002**, *9*, 829−838. (f) Merzlyak, P. G.; Capistrano, M. F. P.; Valeva, A.; Kasianowicz, J. J.; Krasilnikov, O. V. *Biophys. J.* **2005**, *89*, 3059−3070. (g) Kang, X. F.; Cheley, S.; Guan, X. Y.; Bayley, H. *J. Am. Chem. Soc.* **2006**, *128*, 10684−10685.

(4) Lev, A. A.; Korchev, Y. E.; Rostovtseva, T. K.; Bashford, C. L.; Edmonds, D. T.; Pasternak, C. A. *Proc. R. Soc. London, Ser. B* **1993**, *252*, 187−192.

(5) (a) Sun, L.; Crooks, R. M. *J. Am. Chem. Soc.* **2000**, *122*, 12340−12345. (b) Apel, P. Y.; Korchev, Y. E.; Siwy, Z.; Spohr, R.; Yoshida, M. *Nucl. Instrum. Methods Phys. Res., Sect. B* **2001**, *184*, 337−346. (c) Harrell, C. C.; Siwy, Z. S.; Martin, C. R. *Small* **2006**, *2*, 194−198. (d) Wu, S. S.; Park, S. R.; Ling, X. S. *Nano Lett.* **2006**, *6*, 2571−2576.

(6) (a) Shao, Y. H.; Mirkin, M. V. *J. Am. Chem. Soc.* **1997**, *119*, 8103−8104. (b) Zhang, B.; Zhang, Y. H.; White, H. S. *Anal. Chem.* **2004**, *76*, 6229−6238. (c) Umehara, S.; Pourmand, N.; Webb, C. D.; Davis, R. W.; Yasuda, K.; Karhanek, M. *Nano Lett.* **2006**, *6*, 2486−2492.

(7) Li, J.; Stein, D.; McMullan, C.; Branton, D.; Aziz, M. J.; Golovchenko, J. A. *Nature* **2001**, *412*, 166−169.

(8) Storm, A. J.; Chen, J. H.; Ling, X. S.; Zandbergen, H. W.; Dekker, C. *Nat. Mater.* **2003**, *2*, 537−540.

(9) Wu, M. Y.; Krapf, D.; Zandbergen, M.; Zandbergen, H.; Batson, P. E. *Appl. Phys. Lett.* **2005**, *87*, 113106.

(10) Kim, M. J.; Wanunu, M.; Bell, D. C.; Meller, A. *Adv. Mater.* **2006**, *18*, 3149−3153.

(11) Heng, J. B.; Ho, C.; Kim, T.; Timp, R.; Aksimentiev, A.; Grinkova, Y. V.; Sligar, S.; Schulten, K.; Timp, G. *Biophys. J.* **2004**, *87*, 2905−2911.

(12) Fologea, D.; Gershow, M.; Ledden, B.; McNabb, D. S.; Golovchenko, J. A.; Li, J. L. *Nano Lett.* **2005**, *5*, 1905−1909.

(13) Storm, A. J.; Chen, J. H.; Zandbergen, H. W.; Dekker, C. *Phys. Rev. E* **2005**, *71*, 051903.

(14) (a) Siwy, Z. S.; Powell, M. R.; Petrov, A.; Kalman, E.; Trautmann, C.; Eisenberg, R. S. *Nano Lett.* **2006**, *6*, 1729−1734. (b) Siwy, Z.; Kosinska, I. D.; Fulinski, A.; Martin, C. R. *Phys. Rev. Lett.* **2005**, *94*, 048102.

(15) (a) Heins, E. A.; Baker, L. A.; Siwy, Z. S.; Mota, M.; Martin, C. R. *J. Phys. Chem. B* **2005**, *109*, 18400−18407. (b) Heins, E. A.; Siwy, Z. S.; Baker, L. A.; Martin, C. R. *Nano Lett.* **2005**, *5*, 1824−1829.

(16) Siwy, Z.; Trofin, L.; Kohli, P.; Baker, L. A.; Trautmann, C.; Martin, C. R. *J. Am. Chem. Soc.* **2005**, *127*, 5000−5001.

(17) Han, A. P.; Schurmann, G.; Mondin, G.; Bitterli, R. A.; Hegelbach, N. G.; de Rooij, N. F.; Staufer, U. *Appl. Phys. Lett.* **2006**, *88*, 093901.

(18) Mitsui, T.; Stein, D.; Kim, Y. R.; Hoogerheide, D.; Golovchenko, J. A. *Phys. Rev. Lett.* **2006**, *96*, 036102.

(19) (a) Harrell, C. C.; Lee, S. B.; Martin, C. R. *Anal. Chem.* **2003**, *75*, 6861−6867. (b) Polk, B. J.; Bernard, M.; Kasianowicz, J. J.; Misakian, M.; Gaitan, M. *J. Electrochem. Soc.* **2004**, *151*, C559−C566.

(20) (a) Chen, P.; Mitsui, T.; Farmer, D. B.; Golovchenko, J.; Gordon, R. G.; Branton, D. *Nano Lett.* **2004**, *4*, 1333−1337. (b) Danelon, C.; Santschi, C.; Brugger, J.; Vogel, H. *Langmuir* **2006**, *22*, 10711−10715.

(21) Nilsson, J.; Lee, J. R. I.; Ratto, T. V.; Letant, S. E. *Adv. Mater.* **2006**, *18*, 427−431.

(22) Wang, G. L.; Zhang, B.; Wayment, J. R.; Harris, J. M.; White, H. S. *J. Am. Chem. Soc.* **2006**, *128*, 7679−7686.

(23) (a) Giridhar, R. V.; Rose, K. *J. Electrochem. Soc.* **1988**, *135*, 2803−2807. (b) Yanez, J. A.; Baretzky, B.; Wagner, M.; Sigmund, W. M. *J. Eur. Ceram. Soc.* **1998**, *18*, 1493−1502. (c) Waltman, R. J.; Yen, B. K.; White, R. L.; Pocker, D. J. *Chem. Mater.* **2004**, *16*, 4878−4889. (d) Wu, P.; Hogrebe, P.; Grainger, D. W. *Biosens. Bioelectron.* **2006**, *21*, 1252−1263.

(24) Netzer, L.; Sagiv, J. *J. Am. Chem. Soc.* **1983**, *105*, 674−676.

(25) The effective film thickness, calculated from attenuation of the substrate signals, is consistent with the thickness measured by ellipsometry.

(26) http://srdata.nist.gov/xps

(27) Egerton, R. F.; Li, P.; Malac, M. *Micron* **2004**, *35*, 399−409.

(28) (a) Williams, R. A.; Blanch, H. W. *Biosens. Bioelectron.* **1994**, *9*, 159−167. (b) Rozkiewicz, D. I.; Kraan, Y.; Werten, M. W. T.; de Wolf, F. A.; Subramaniam, V.; Ravoo, B. J.; Reinhoudt, D. N. *Chem. Eur. J.* **2006**, *12*, 6290−6297.

(29) Stein, D.; Kruithof, M.; Dekker, C. *Phys. Rev. Lett.* **2004**, *93*, 035901.

(30) (a) Schiedt, B.; Healy, K.; Morrison, A. P.; Neumann, R.; Siwy, Z. *Nucl. Instrum. Methods Phys. Res., Sect. B* **2005**, *236*, 109−116. (b) Daiguji, H.; Yang, P. D.; Majumdar, A. *Nano Lett.* **2004**, *4*, 137−142. (c) Ramirez, P.; Aguilella-Arzo, M.; Alcaraz, A.; Cervera, J.; Aguilella, V. M. *Cell Biochem. Biophys.* **2006**, *44*, 287−312.

(31) (a) Kakiuchi, T.; Iida, M.; Imabayashi, S.; Niki, K. *Langmuir* **2000**, *16*, 5397−5401. (b) Nishiyama, K.; Kubo, A.; Ueda, A.; Taniguchi, I. *Chem. Lett.* **2002**, 80−81.

(32) (a) Goyne, K. W.; Zimmerman, A. R.; Newalkar, B. L.; Komarneni, S.; Brantley, S. L.; Chorover, J. *J. Porous Mater.* **2002**, *9*, 243−256. (b) Duval, Y.; Mielczarski, J. A.; Pokrovsky, O. S.; Mielczarski, E.; Ehrhardt, J. J. *J. Phys. Chem. B* **2002**, *106*, 2937−2945.

(33) Wang, A. F.; Tang, H. Y.; Cao, T.; Salley, S. O.; Ng, K. Y. S. *J. Colloid Interface Sci.* **2005**, *291*, 438−447.

NL070462B